Healing of oxygen vacancies on reduced surfaces of gold-doped ceria

Michael Nolan

Citation: The Journal of Chemical Physics **130**, 144702 (2009);
View online: https://doi.org/10.1063/1.3110702
View Table of Contents: http://aip.scitation.org/toc/jcp/130/14
Published by the American Institute of Physics

Healing of oxygen vacancies on reduced surfaces of gold-doped ceria

Michael Nolan[a)]
Tyndall National Institute, Lee Maltings, Prospect Row, Cork, Ireland

(Received 10 December 2008; accepted 10 March 2009; published online 8 April 2009)

As an oxidation-reduction catalyst, ceria can catalyze molecular oxidation and reduction. There has been a focus on understanding and enhancing the vacancy formation process to improve the oxidative power of ceria. However, it is important to also address healing of the surface vacancy. To investigate healing of oxygen vacancies in ceria, we study the interaction of atomic and molecular oxygen and NO_2 with oxygen vacancies on gold-doped (110) and (100) surfaces using density functional theory, corrected for on-site Coulomb interactions (DFT+U). For atomic and molecular oxygen, adsorption at the reduced surface is favorable and results in an oxygen atom sitting in an oxygen lattice site, healing the oxygen vacancy. On undoped surfaces, O_2 adsorbs as a peroxo (O_2^{2-}) species. However, on the doped (110) surface a superoxo (O_2^{-}) species is present. When NO_2 adsorbs (exothermically) at a divacancy surface, one oxygen of the molecule sits in the vacancy site and the N–O distances are elongated and an $[NO_2]^-$ anion forms, similar to the undoped surface. Vacancy healing of ceria surfaces is favorable, even if vacancy formation is enhanced, justifying the current focus on improving the oxidative power of ceria. We briefly examine a catalytic cycle: the reaction of CO with adsorbed O_2 on the undoped and doped surfaces, and find that the doped (110) surface facilitates CO oxidation. © *2009 American Institute of Physics*. [DOI: 10.1063/1.3110702]

I. INTRODUCTION

Cerium dioxide (ceria) is a widely studied oxidation-reduction catalyst[1–4] and is of interest as a metal oxide gas sensor. In both applications, the key to the activity of ceria is generally attributed to the ease with which oxygen vacancies are formed, which has its origin in the ability of cerium to change oxidation state from (formally) +4 to (formally) +3. A well-known example of an oxidation-reduction (redox) catalytic cycle on ceria is CO oxidation and NO_X reduction. In simple terms, the redox scheme involves CO abstracting oxygen from the oxide surface, forming CO_2 and an oxygen vacancy at the surface. The vacancy can be healed by an NO_X molecule giving up an oxygen atom or by oxygen present in the atmosphere. Another possible catalytic cycle is that an oxygen molecule heals the vacancy and one of the oxygen atoms can be used to oxidize CO.

To enhance the oxidative power of the oxide, it should ideally display a relatively small oxygen vacancy formation energy. However, enhancing the oxidative power should not hurt vacancy healing. This would mean, for example, that NO_X reduction would not be impaired. In the literature to date, only reduction of ceria has been widely studied, e.g., Refs. 5–11. Less attention has been given to the process of oxygen vacancy healing. Two recent papers are of interest for vacancy healing with oxygen.[12,13] Huang and Fabris[12] studied atomic and molecular oxygen adsorption at the undoped stoichiometric (111) and (110) surfaces and the reduced (111) surface using first principles density functional theory (DFT) corrected for on-site Coulomb interactions, DFT+U, which has previously been applied to reduced ceria.[6–8,11] Choi *et al.*[13] presented a combined Raman spectroscopy and theoretical study of oxygen interaction with the stoichiometric and reduced (111) surface. In both studies, atomic and molecular oxygen interact weakly with nondefective surfaces, forming a tilted peroxo (O_2^{2-}) unit, with an elongated O–O bond. On the defective (111) surface, atomic and molecular oxygen exothermically reoxidize the vacancy site. Two signals were observed in the Raman spectrum of Ref. 13 at 825 and 1131 cm^{-1}, characteristic of peroxo and superoxo (O_2^{-}) species. In the computations, the most stable adsorption site is that in which one oxygen atom sits in the vacancy site, forming a peroxo species, with an O–O bond length of 1.43 Å and a stretching frequency of 972 cm^{-1}. These findings were consistent with experiment, although the stretching frequency was overestimated. The superoxo adsorption structure was only 0.05 eV less stable.

Studies of NO/NO_2 reduction have focused more on the fate of the molecule during the reduction process[14–16] and establishing a reaction mechanism. NO_X reduction can produce N_2, as well as a number of more complex products, such as NO_3 or N_2O.[14,15] For NO_X oxidation, we have previously studied NO_2 adsorption at undoped defective (111), (110), and (100) ceria surfaces[16] using DFT+U and found that reoxidation of the oxide surface, with transfer of an electron to NO_2, forming an NO_2^- anion, is favorable. Yang *et al.* studied NO reduction at the (110) surface with standard DFT (Ref. 17) and found that two NO molecules adsorbed at a surface with two vacancies starts to dissociate.

Doping of ceria with elements, such as Zr or Au, promotes catalytic activity for oxidation reactions[5,10,18–21] by enhancing vacancy formation.[5,10,18–21] Recently, we have shown that Au doping of ceria surfaces, where the dopant is incorporated into the surface layer, gives rise to reduced oxygen vacancy formation energies.[10,21] However, there is also a need to study the healing of oxygen vacancies in the doped surface, which has yet to be addressed and is the subject of

[a)]Electronic mail: michael.nolan@tyndall.ie.

the present paper. We also consider a catalytic cycle, which involves oxidation of CO using an oxygen atom from adsorbed O_2, and show how this reaction is affected by the surface structure and doping.

We use DFT corrected for on-site Coulomb interactions (DFT+U) to describe reduced Ce ions in the (110) and (100) surfaces[6–8,11,19,21–27] and study the interaction of atomic and molecular oxygen and NO_2 with Au-doped (110) and (100) ceria surfaces. Each doped surface carries two oxygen vacancies. This is because the first oxygen vacancy forms spontaneously upon Au doping of the surface[21] and it is the second oxygen vacancy that is active. We find that O and O_2 adsorb exothermically, healing vacancy sites. The exact structure that results upon adsorption of O_2 depends on the surface; when both surfaces are undoped, a peroxo species is found, but on the doped surfaces, a superoxo species is formed on (110) and a peroxo species on the (100) surface. When NO_2 adsorbs exothermically on both surfaces, the molecule starts to dissociate, and the surfaces are partially reoxidized. Compared to the undoped surface, the energy gain upon vacancy healing is smaller. These results, along with those of Ref. 16 show that healing of oxygen vacancies on ceria is favorable and the most important reaction in ceria redox catalysis is the formation of the active oxygen vacancy.

II. METHODS

We use a slab to describe the ceria surfaces and a plane wave basis set to describe the wave functions of the valence electrons.[28] The converged plane wave cutoff energy is 396 eV; in Refs. 6 and 7 convergence tests for the technical parameters discussed below are discussed. The projector augmented wave approach[29] describes the interaction between the core and the valence electrons. Ce is described with 12 valence electrons; a [He] core is used for C, N, and O and a [Xe] core on Au. The Perdew–Burke–Ernzerhof functional[30] accounts for exchange and correlation. In common with other works,[6–8,11,19,21–27] we use DFT corrected for on-site Coulomb interactions (DFT+U). $U=5$ eV and is applied to the Ce 4f states. The details of this approach and the choice of U are discussed extensively in Refs. 6–8, 11, 19, and 21–27. Briefly, the self-interaction of an electron is not correctly canceled in DFT resulting in an artificial barrier to electronic localization, since self-interaction is biased toward delocalizing electronic states. The introduction of the on-site Coulomb interaction U removes some of the self-interaction error, reducing the localization barrier, allowing formation of localized electronic states, in agreement with experiment and contrary to the generalized gradient approximation description. The value of U is chosen to recover the correct value of an experimentally measured parameter, e.g., the magnetic moment or the band gap. For defective systems, this is difficult and our strategy has been to choose a value of U that leads to localization of two electrons in the Ce 4f states for each oxygen vacancy and an electronic structure corresponding to that observed in experimental ultraviolet photoemission spectroscopy (UPS) spectra.[6,7,31,32] k-point sampling is performed using the Monkhorst–Pack scheme, with a $(2\times2\times1)$ grid, and Fermi level smearing is performed using the Methfessel–Paxton scheme.[33]

The (110) surface is a type I surface,[6,34] with neutral atomic planes. The (100) surface is a type III surface with a nonzero dipole moment. Moving half of the oxygen atoms from one face of the slab to the other removes the dipole.[6,35] For the (110) and (100) surfaces thicknesses of 11.5 Å (seven atomic layers) and 10.94 Å (nine atomic layers) were required. The vacuum layer is 15 Å on both surfaces. For the (110) surface a (2×2) expansion of the surface unit cell gives eight surface oxygen atoms, while for the (100) surface, a (4×2) expansion of the surface unit cell is used, the same as in Ref. 21. Upon introduction of the dopant, a vacancy, and an adsorbate, the ions in all layers, except the bottom two, are relaxed. For the ionic relaxation in a fixed lattice, the forces are relaxed until they are less than 0.02 eV/Å.

Atomic and molecular oxygen and NO_2 are adsorbed at surface oxygen vacancy sites and the surface-adsorbate structures are relaxed with fixed lattice constants. All calculations are spin polarized and allowed to relax to their most favorable spin solution. The energetics and the geometry of the gas phase molecules are calculated at the Γ point, with the unit cells from both surfaces and from a $12\times12\times12$ Å^3 cell; the latter cell guarantees that the molecules are separated and comparing with the supercell from the surface calculations, the differences in energy between the two cells are minimal. Vibrational frequencies for the adsorbates are computed by numerical differencing of the forces to generate a second derivative matrix in a fixed lattice. Diagonalization of the mass weighted matrix gives rise to vibrational frequencies and atomic displacements.

III. RESULTS

A. Doped surfaces

We briefly recap our results for vacancy formation in Au-doped ceria surfaces. In Fig. 1, we show the atomic structures for the Au-doped (110) and (100) surfaces with two oxygen vacancies in their most stable configurations.[21] In each figure, the dopant is the gray sphere in the outermost layer of Ce atoms in each surface and the vacancy sites are indicated with a blue "V." Upon relaxation of the doped surfaces, there are some structural changes in the surface structures, e.g., the surface layer atoms in the (110) surface near the dopant move out of the surface plane and in the (100) surface, the oxygen atoms around the dopant site are also distorted off their lattice sites. When oxygen vacancies form on each surface, there are strong changes to the surface structure. These are discussed in more detail in Ref. 21.

Formation of the first oxygen vacancy on each surface has a negative energy, meaning that oxygen vacancies will be present at 0 K in the absence of gas phase oxygen. Therefore, we work from the premise that formation of a second oxygen

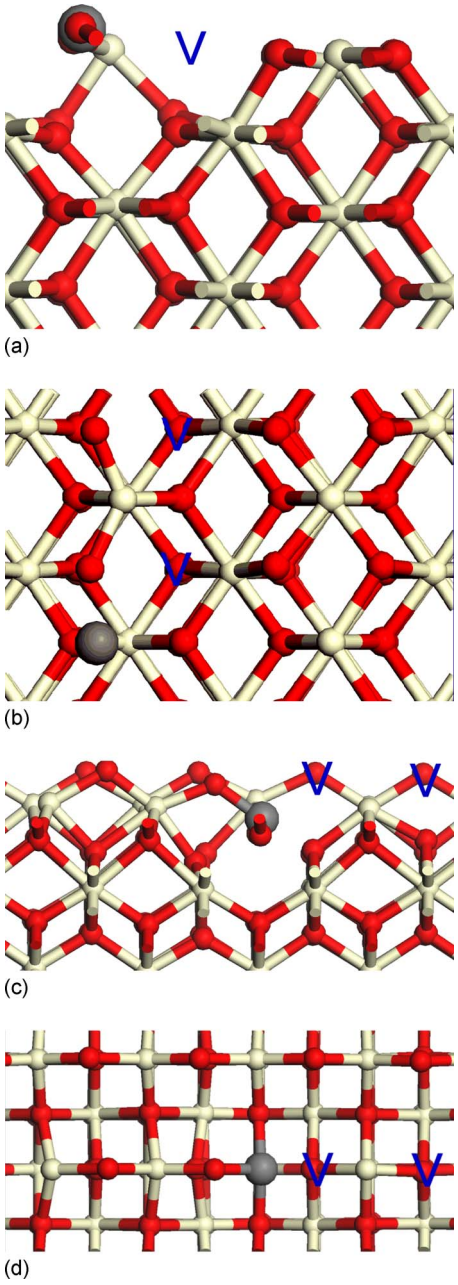

FIG. 1. (Color online) Surface structures of ceria doped with Au. [(a) and (b)] (110) surface with two oxygen vacancies. [(c) and (d)] (100) surface with two oxygen vacancies. The dopant is the large gray sphere and Ce is white and O is red. The vacancy sites are denoted with a blue V and in the view of part (a) the vacancies lie on a line so that only one vacancy symbol appears.

vacancy determines the activity of the doped surface. The vacancy formation energy on the (110) surface with the vacancy pattern in Fig. 1 is +0.68 eV, while on (100), the corresponding oxygen vacancy has a formation energy of +2.57 eV. Compared with the undoped surface, where the vacancy formation energies are 1.99 and 2.10 eV,[6,7] we see that formation of the second vacancy on (110) is rather easy, whereas on (100), doping makes little difference to the formation of the catalytically active vacancy. In all defective surfaces, the Ce electronic density of states shows formation of reduced Ce^{3+} ions, similar to oxygen vacancy formation on the undoped surfaces.[21]

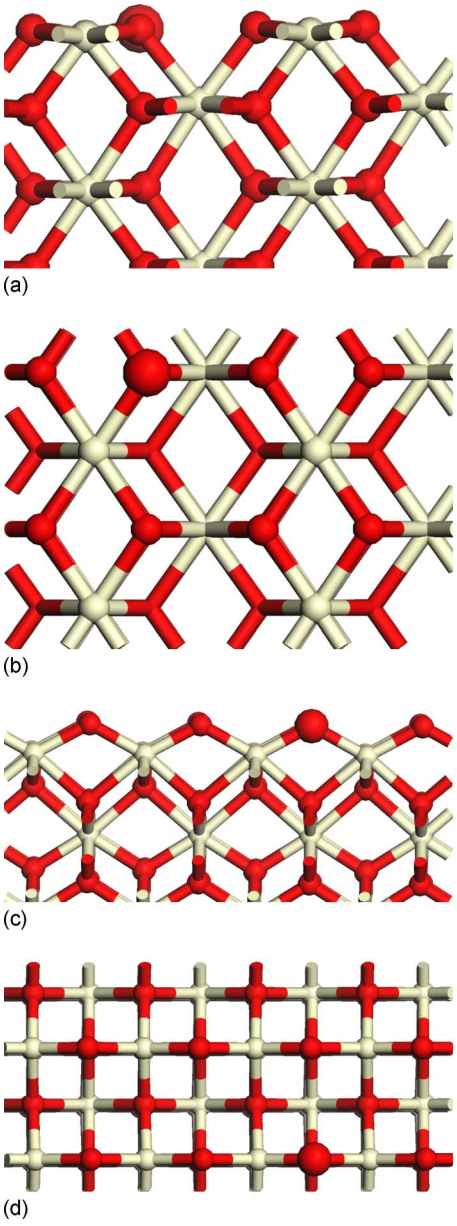

FIG. 2. (Color online) Adsorption structures for atomic O adsorbed at the [(a) and (b)] undoped (110) surface and [(c) and (d)] (100) surface of ceria. The adsorbed oxygen atom is the large red sphere.

B. O/O_2 adsorption on the defective undoped (110) and (100) surfaces

In this section, we investigate adsorption of atomic and molecular oxygen on the defective, undoped (110) and (100) surfaces with one oxygen vacancy. The adsorption structures for atomic oxygen are shown in Fig. 2 and for molecular oxygen in Fig. 3. In both figures, the large red spheres show the oxygen atoms of adsorbed atomic O and molecular O_2; in both cases, oxygen is found at the vacancy site. The energy change upon adsorption of O/O_2 is given by

$$E^{\mathrm{ads}} = E(\mathrm{CeO_{2\text{-}2Ovac}} - \mathrm{O}) - \left[E(\mathrm{CeO_{2\text{-}2Ovac}}) + \tfrac{1}{2}E(\mathrm{O_2})\right], \tag{1}$$

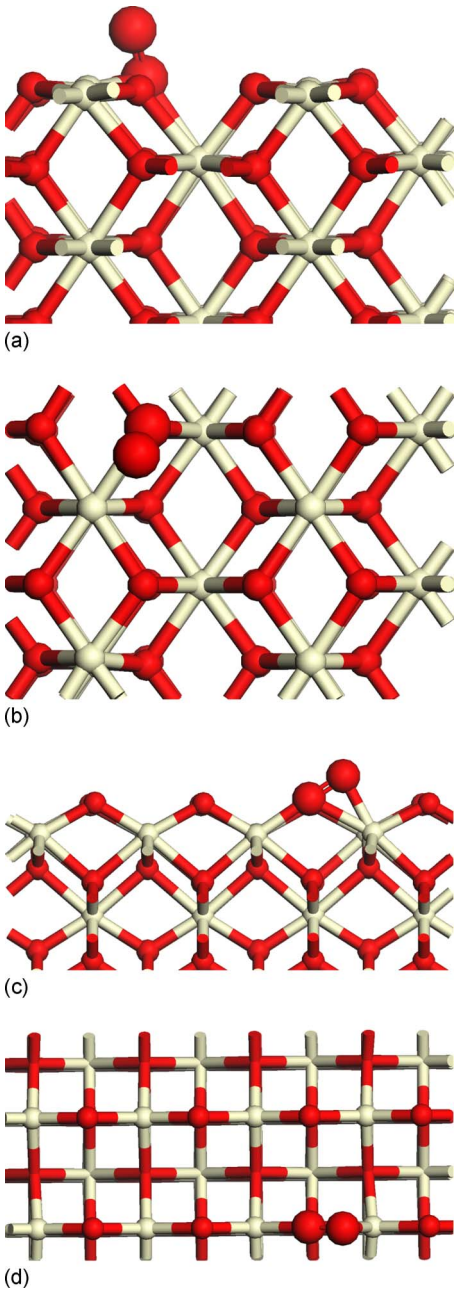

FIG. 3. (Color online) Adsorption structures for molecular O_2 adsorbed at the [(a) and (b)] undoped (110) surface and [(c) and (d)] (100) surface of ceria. The adsorbed oxygen atoms are the large red spheres.

$$E^{\text{ads}} = E(\text{CeO}_{2\text{-}2\text{Ovac}} - \text{O}_2) - [E(\text{CeO}_{2\text{-}2\text{Ovac}}) + E(\text{O}_2)], \quad (2)$$

where $CeO_{2\text{-}2Ovac}$ is the defective surface with two oxygen vacancies [1.8% vacancy concentration in the (110) surface and 1.6% vacancy concentration in the (100) surface] and $CeO_{2\text{-}2Ovac}$–O and $CeO_{2\text{-}2Ovac}$–O_2 signify the defective surfaces with adsorbed atomic and molecular oxygen, respectively. In Eqs. (1) and (2), a negative adsorption energy signifies a stabilization upon adsorption.

When an oxygen atom adsorbs at the vacancy site on both surfaces it heals the vacancy, with adsorption energies of −2.07 eV for the (110) surface and −2.22 eV for the (100) surface. Since the oxygen atom heals the vacancy site, it is no surprise that the above adsorption energies are essentially the negative of the vacancy formation energy on the undoped surfaces,[7] since vacancy healing with an oxygen atom reverses the formation of the vacancy.

When O_2 adsorbs at both surfaces, one oxygen atom sits in the previous vacancy site, with adsorption energies of −2.05 eV on (110) and −2.02 eV on (100). Again, an oxygen atom heals the vacancy site; the presence of the other oxygen atom in the O_2 molecule has a small influence on the exact position of the adsorbed oxygen atom, which is reflected in the smaller adsorption energies. The O–O bond is elongated from 1.20 Å in the gas phase molecule to 1.44 Å on (110) and 1.42 Å on (100), indicating that the molecule is dissociating. The O–O computed stretching frequencies are 900 cm^{-1} on (110) and 885 cm^{-1} on (100). These data are consistent with formation of a peroxo species upon O_2 adsorption at both surfaces, which was also found to be present on the (111) surface.[12,13]

C. O/O_2 adsorption on the defective doped (110) and (100) surfaces

In this section, we consider adsorption of atomic and molecular oxygen at the defective doped surfaces and compare with the undoped surfaces. We have examined possible adsorption sites on each surface, with the most stable adsorption sites shown in Fig. 4 for atomic oxygen adsorption and Fig. 5 for molecular oxygen adsorption; the adsorbed oxygen atom(s) is (are) indicated as large red spheres. The computed adsorption energies for O and O_2 adsorption at the undoped and Au-doped defective surfaces are given in Table I. Adsorption of O and O_2 on the doped surfaces is exothermic. The gain in energy upon surface reoxidation is lower on the doped (110) surface compared to the undoped surface, while on the (100) surface, the energy gain is similar to the undoped surface. On (110), this finding is consistent with the fact that oxygen vacancy formation is enhanced when it is doped[21] and thus vacancy healing will be less favorable, while on the (100) surface, the opposite is found. However, all energies are negative, indicating that partial reoxidation of a doped ceria surface with two oxygen vacancies will still be possible. This makes the Au-doped (110) surface a potentially useful catalyst for redox reactions. The energetics of the (100) surface do not make it as potentially useful, there being little improvement in the vacancy formation energy upon doping.[21]

For atomic O adsorption at both doped surfaces, the oxygen is in a vacancy site. In the (110) surface, this site is in the surface layer, with a distance of 2.06 Å to the nearest surface Ce ion. The remainder of the geometry in the surface lattice is little affected by the presence of this oxygen atom, since the surface is already distorted upon doping. On the (100) surface, the distance from the adsorbed oxygen to the nearest Ce atom is 2.0 Å and the surface geometry is similar to that of the defective doped surface discussed in Ref. 21.

For O_2 adsorption at both surfaces one oxygen atom is also found in a vacancy site, healing the oxygen vacancy, and the second oxygen atom points out of the surface plane. On the doped (110) surface, the O–O bond of O_2 is elongated to

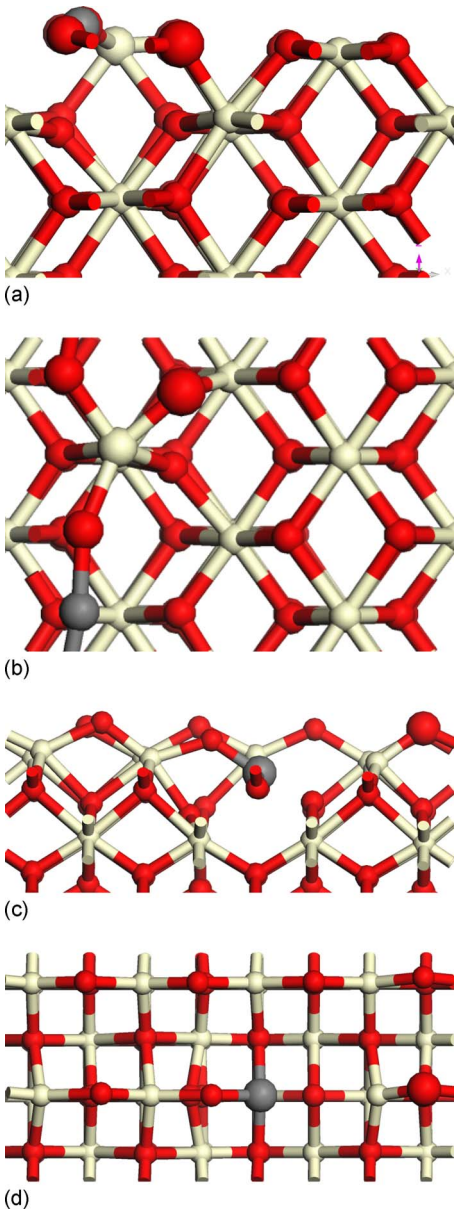

FIG. 4. (Color online) Adsorption structures for atomic O adsorbed at the [(a) and (b)] doped (110) surface and [(c) and (d)] doped (100) surface of ceria. The adsorbed oxygen atom is the large red sphere.

1.34 Å compared to 1.20 Å for the gas phase molecule and 1.44 Å on the undoped surface. Thus, upon adsorption, O_2 starts to dissociate; however the elongation of the O–O bond on the doped (110) surface is less pronounced than on the undoped surface. The computed O–O stretch is 1135 cm^{-1}. This stretch and the O–O distance indicate formation of a superoxo species at the doped (110) surface, compared to a peroxo species at the undoped surface. We attribute this change in the nature of the adsorbed species to the fact that this surface prefers to form a vacancy, so that healing the vacancy will be harder and hence it is less favorable for the oxide to transfer charge to the O_2 molecule thus lengthening the O–O bond and reoxidizing the surface.

On the (100) surface, the O–O bond elongates to 1.47 Å, compared to 1.42 Å on the undoped surface, with a computed O–O stretching frequency of 966 cm^{-1}. This indicates formation of a peroxo species at the doped (100) surface.

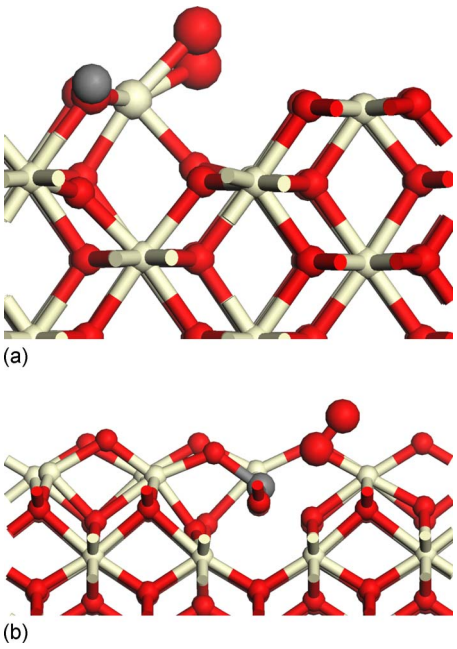

FIG. 5. (Color online) Adsorption structures for molecular O_2 adsorbed at the (a) doped (110) surface and (b) doped (100) surface of ceria. The adsorbed oxygen atom is the large red sphere.

This is in contrast to the (110) surface and has a similar origin in the favorability of vacancy formation versus vacancy healing. From Refs. 12 and 13 O_2 adsorption at the undoped (111) surface leads to formation of a peroxo species. This dependence of oxygen adsorption on the orientation and structure of the ceria surface is not surprising; the strong surface dependence for, e.g., CO oxidation on ceria surfaces is well known.[36–38]

D. NO_2 adsorption at the defective doped surface

In Sec. III C, the adsorption of oxygen was presented as one model of vacancy healing in the presence of oxygen from the atmosphere. A further model is to examine the redox catalytic cycle, in which ceria facilitates oxidation of CO and is reoxidized by reduction of an NO_2 molecule. It is the latter reaction on doped ceria surfaces that we study in this section. In a previous study,[16] we investigated NO_2 adsorption at undoped, reduced ceria surfaces and found that NO_2 adsorbs at a vacancy site, with transfer of an electron from the surface to the adsorbate, forming an $[NO_2]^-$ anion; the anion shows one elongated N–O bond, indicating the onset of molecular dissociation to NO and an oxygen, and it is the latter oxygen that heals the vacancy site.

TABLE I. Adsorption energies (E^{ads}) for adsorption of atomic and molecular oxygen at the undoped and Au-doped (110) and (100) surfaces with two oxygen vacancies.

Surface	Atomic oxygen E^{ads} (eV)	Molecular oxygen E^{ads} (eV)
Undoped (110)	−2.07	−2.05
Doped (110)	−0.62	−1.20
Undoped (100)	−2.22	−2.02
Doped (100)	−2.23	−2.68

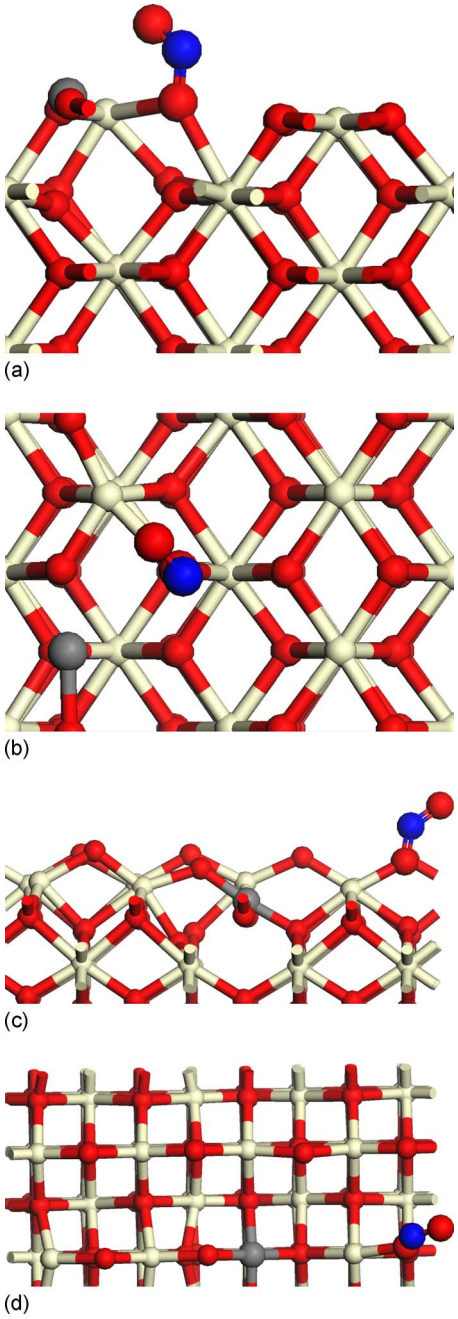

FIG. 6. (Color online) Adsorption structures for NO_2 adsorbed at divacancy surfaces: [(a) and (b)] (110) surface and [(c) and (d)] (100) surface. The color scheme is the same as in Fig. 1, with the N atom colored blue and the larger spheres indicating the atoms of NO_2.

In the present investigation, the NO_2 molecule is initially adsorbed with one oxygen atom at a vacancy site. The energy change upon adsorption of NO_2 on a surface with two oxygen vacancies is given by

$$E^{\text{ads}} = E(\text{CeO}_{2\text{-}2\text{Ovac}} - \text{NO}_2) - [E(\text{CeO}_{2\text{-}2\text{Ovac}}) + E(\text{NO}_2)]. \quad (3)$$

The adsorption energy on the Au-doped (110) surface is −1.46 eV (−2.25 eV on the undoped surface[16]) and on the Au-doped (100) surface it is −1.97 eV (−2.23 eV on the undoped surface[16]). The surface with the most favorable vacancy formation energy, i.e., (110), shows the least favorable (smallest) NO_2 adsorption energy. Compared to the undoped surface, doping reduces the adsorption energies and this is more pronounced on the (110) surface. However, the fact that the adsorption energies are negative indicates that doping has no deleterious effect on this aspect of the surface-molecule interaction–that is, the fact that the molecule will adsorb at the surface and use one of its oxygen atoms to heal the vacancy site.

The relaxed structures for adsorbed NO_2 are shown in Fig. 6. The oxygen atom in adsorbed NO_2 found at the oxide surface is denoted O_S and the other oxygen is denoted O_N. On the (110) surface, the $N-O_S$ and $N-O_N$ distances are 1.30 and 1.26 Å, compared to 1.20 Å in gas phase NO_2 and NO. On (100), the same distances are 1.30 and 1.27 Å. Thus structural changes in the molecule upon adsorption, i.e., the lengthening of both N–O distances, with a larger elongation involving O_S, are the same on both surfaces. On the undoped (110) surface,[16] we found that the $N-O_S$ bond elongates to 1.31 Å and on (100), this bond elongates to 1.44 Å, with the $N-O_N$ bond changed to 1.25 and 1.19 Å on the undoped (110) and (100) surfaces, respectively.

In Fig. 7 we show the Ce 4*f*, N 2*p*, and O 2*p* projected electronic density of states (PEDOS) for NO_2 adsorbed at the Au-doped (110) and (100) surfaces. The Ce PEDOS shows occupied Ce 4*f* states, indicating that reduced Ce^{3+} ions are present.[6–8] The interesting aspect of the PEDOS is that of the adsorbed molecule, which is very different to that for gas phase NO_2. The latter is a radical with one unpaired electron, so that the up spin and down spin PEDOSs are different (see Ref. 16, Fig. 4). In Fig. 7, the PEDOS shows spin pairing (up and down spin PEDOSs are the same) as well as different peak positions and shapes compared to NO_2. These PEODS plots are very similar to those found for NO_2 adsorbed at the same undoped surfaces[16] and are consistent with formation of reduced $[NO_2^-]$, which results from transfer of charge from a Ce^{3+} ion at surface to the adsorbate, thus reducing NO_2 and helping in reoxidation of the defective surface.

E. A catalytic cycle: CO oxidation

To investigate the impact of surface structure and doping on a catalytic cycle, we consider briefly the reaction of CO at the undoped and doped surfaces with adsorbed O_2 from Secs. III B and III C. This model was discussed in Sec. I and has been studied for the (111) surface in Ref. 10. On the undoped (110) surface, CO interacts weakly with the O_2-adsorbed surface, leaving intact CO and surface peroxide, with a small energy gain of −0.12 eV, Fig. 8(a). If we calculate the energy for CO_2 formation, leaving a healed surface, there is a gain of −3.40 eV. However, there must be a barrier to this reaction since it does not take place during the calculations. On the doped (110) surface, the situation is rather different. In this case, CO reacts directly with O_2 and abstracts an oxygen atom, forming CO_2 and a healed surface, shown in Fig. 8(b); no intermediate $(CO)_3$ species is found in this case. The energy gain for this reaction is −2.53 eV over separated CO and the O_2-adsorbed surface, indicating a driving force toward CO oxidation and surface reoxidation. Thus, the role of doping in enhancing molecular oxidation at this ceria sur-

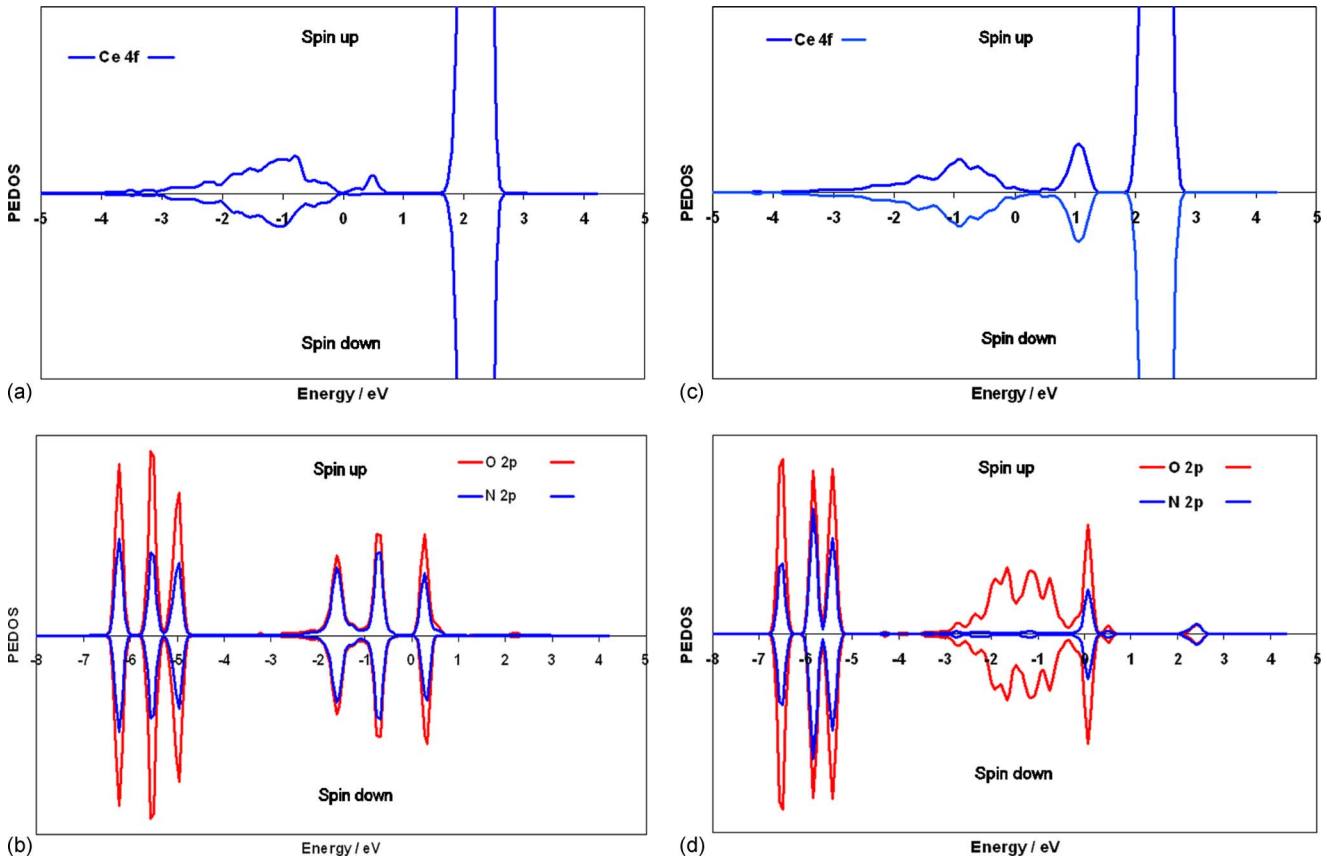

FIG. 7. (Color online) (a) Ce 4*f* PEDOS for NO_2 adsorbed on the Au-doped (110) surface, (b) N and O 2*p* PEDOS for NO_2 adsorbed on the Au-doped (110) surface, (c) Ce 4*f* PEDOS for NO_2 adsorbed on the Au-doped (100) surface, and (d) N and O 2*p* PEDOS for NO_2 adsorbed on the Au-doped (100) surface

face is seen clearly and our results indicate the potential utility of structures exposing the (110) surface for improved oxidation catalysts.

On the undoped (100) surface, CO and surface O_2 do not react; the energy gain is only −0.10 eV, with the structure shown in Fig. 8(c). On the Au-doped (100) surface, CO interacts with the oxygen atoms of adsorbed O_2 to form a $(CO)_3$ species at the surface, similar to the undoped surface.[38] There is an energy gain of −4.43 eV and the adsorption structure is shown in Fig. 8(d). The geometry of the adsorbate shows C–O distances of 1.20 Å (C–O pointing out of the surface) and 1.35/1.37 Å (to oxygen at the surface), consistent with formation of a carbonatelike group at this surface; see Ref. 38. There is no direct formation of CO_2.

These finding are consistent with previous work comparing the two surfaces[38]—where we found that the doped (110) surface is more reactive for molecular oxidation, vacancy formation, and CO adsorption than the doped (100) surface. These differences can be easily understood through the atomic structure of the two surfaces, as discussed in Ref. 38.

IV. CONCLUSIONS

The oxidative power of a metal oxide can be described by the oxygen vacancy formation energy, which can be enhanced by cation doping. However, doping should not adversely impact healing of the vacancy, which would limit the usefulness of the oxide as a redox catalyst. To investigate how oxide doping impacts the healing of oxygen vacancies in ceria, we have studied adsorption of atomic and molecular oxygen at the undoped and Au-doped (110) and (100) surfaces of ceria and adsorption of NO_2 at the same surfaces.

Adsorption of atomic oxygen heals a surface oxygen vacancy on undoped and doped surfaces. The adsorption of O_2 heals an oxygen vacancy and the nature of the surface adsorbate depends on the surface and doping. On undoped (110) and (100), a peroxo adsorbate structure is found. In contrast, on the doped (110) surface a superoxo adsorbate structure is present. With different O–O stretching frequencies, these surface-adsorbate structures should be readily discriminated by an experimental technique such as infrared or Raman spectroscopy.

NO_2 adsorbs at a vacancy site on the doped surfaces, so that one oxygen atom heals the vacancy. There is an accompanying change of N–O distances and formation of reduced $[NO_2]^-$, indicating the onset of dissociation of the adsorbed molecule. The presence of a Ce 4*f* derived gap state in the Ce density of states indicates that the surface is partially reoxidized.

The interaction of CO with adsorbed O_2 depends on the surface—at undoped surfaces, there is no reaction, while on doped surfaces, (110) shows CO_2 formation and (100) shows carbonate formation. This indicates an enhancement of CO oxidation at the doped (110) surface of ceria and demonstrates the dramatic impact of ceria doping on the catalytic cycle.

Comparing vacancy healing on undoped and doped, sur-

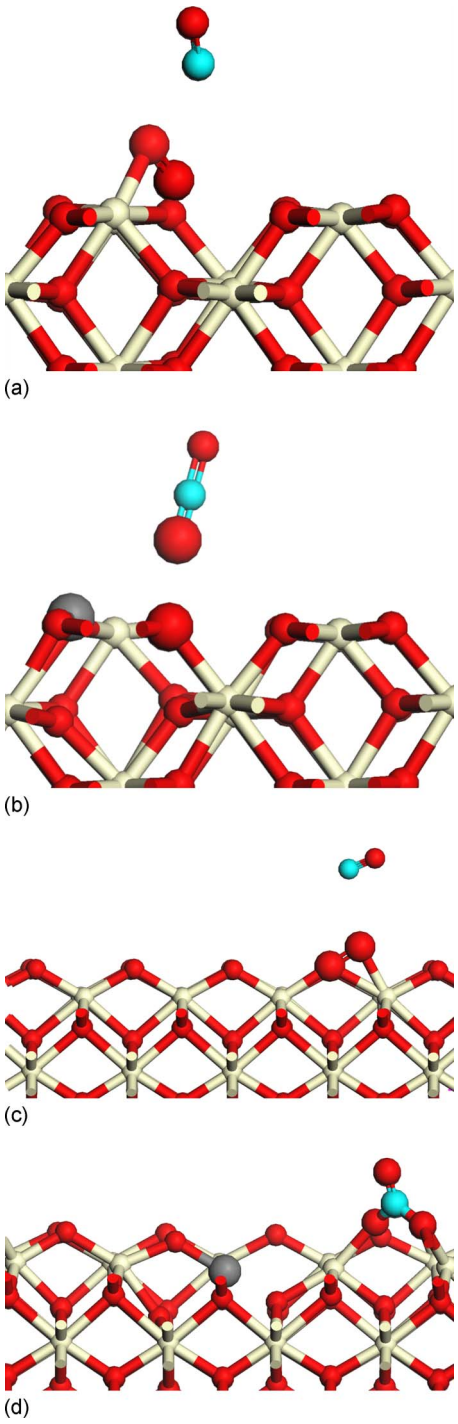

FIG. 8. (Color online) Adsorption structures for CO interacting with O_2-adsorbed ceria surfaces. (a) undoped (110) surface, (b) doped (110) surface, (c) undoped (100) surface, and (d) doped (100) surface. The large red spheres indicate the oxygen atoms of adsorbed O_2 and the cyan spheres the carbon atoms of adsorbed CO.

faces, we find that irrespective of doping, ceria surfaces will undergo vacancy healing, which means that the key step in the activation of ceria is the formation of the active oxygen vacancy, which justifies the large amount of effort expended in this field. Investigations of how cation dopants impact the vacancy formation energy will shed further light on which dopants can be used to improve the activity of ceria in catalysis.

ACKNOWLEDGMENTS

We acknowledge the European Commission for support (NATCO, Grant No. FP6-511925 and REALISE, Grant No. FP6-16172). We acknowledge the Science Foundation Ireland (SFI) funded computing resources at Tyndall and the SFI/Higher Education Authority funded Irish Centre for High End Computing (ICHEC) for provision of computing resources. Professor Horia Metiu is thanked for his interest in this work.

[1] A. Trovarelli, *Catalysis by Ceria and Related Materials* (Imperial College Press, UK, 2002).
[2] A. Trovarelli, Catal. Rev. - Sci. Eng. **38**, 439 (1996).
[3] A. Mehta, S. Patil, H. Bang, H. J. Cho, and S. Seal, Sens. Actuators, A **134**, 146 (2007).
[4] N. Izu, W. Shin, I. Matsubara, and N. Murayama, J. Electroceram. **13**, 703 (2004).
[5] G. Balducci, M. Saiful Islam, J. Kaspar, P. Fornasiero, and M. Graziani, Chem. Mater. **12**, 677 (2000).
[6] M. Nolan, S. Grigoleit, D. C. Sayle, S. C. Parker, and G. W. Watson, Surf. Sci. **576**, 217 (2005).
[7] M. Nolan, S. C. Parker, and G. W. Watson, Surf. Sci. **595**, 223 (2005).
[8] S. Fabris, S. de Gironcoli, S. Baroni, G. Vicario, and G. Balducci, J. Phys. Chem. B **109**, 22860 (2005).
[9] T. X. T. Sayle, S. C. Parker, and D. C. Sayle, Phys. Chem. Chem. Phys. **7**, 2936 (2005).
[10] V. Shapovalov and H. Metiu, J. Catal. **245**, 205 (2007).
[11] M. V. Ganduglia-Pirovano, J. L. F. da Silva, and J. Sauer, Phys. Rev. Lett. **102**, 026101 (2009).
[12] M. Huang and S. Fabris, Phys. Rev. B **75**, 081404 (2007).
[13] Y. M. Choi, H. Abernathy, H. T. Chen, M. C. Lin, and M. L. Liu, ChemPhysChem **7**, 1957 (2006).
[14] M. O. Symalla, A. Drochner, H. Vogel, S. Philipp, U. Gobel, and W. Muller, Top. Catal. **42**, 199 (2007).
[15] U. Berner, K. Schierbaum, G. Jones, P. Wincott, S. Haq, and G. Thornton, Surf. Sci. **467**, 201 (2000).
[16] M. Nolan, S. C. Parker, and G. W. Watson, J. Phys. Chem. B **110**, 2256 (2006).
[17] Z. X. Yang, T. K. Woo, and K. Hermansson, Surf. Sci. **600**, 4953 (2006).
[18] D. A. Andersson, S. I. Simak, N. V. Skorodumova, I. A. Abrikosov, and B. Johansson, Appl. Phys. Lett. **90**, 031909 (2007).
[19] Z. Yang, Z. Lu, G. Luo, and K. Hermansson, Phys. Lett. A **369**, 132 (2007).
[20] G. Dutta, U. V. Waghmare, T. Vaidya, M. S. Hegde, K. R. Priolkar, and P. R. Sarode, Catal. Lett. **108**, 165 (2006).
[21] M. Nolan, V. Soto, and H. Metiu, Surf. Sci. **602**, 2734 (2008).
[22] S. Fabris, S. de Gironcoli, S. Baroni, G. Vicario, and G. Balducci, Phys. Rev. B **71**, 041102 (2005).
[23] J. L. F. da Silva, M. V. Ganduglia-Pirovano, J. Sauer, V. Bayer, and G. Kresse, Phys. Rev. B **75**, 045121 (2007).
[24] C. Loschen, A. Migani, S. T. Bromley, F. Illas, and K. M. Neyman, Phys. Chem. Chem. Phys. **10**, 5730 (2008).
[25] X. Z. Yang, G. X. Luo, Z. S. Luo, T. K. Woo, and K. Hermansson, J. Phys.: Condens. Matter **20**, 035210 (2008).
[26] H. T. Chen, Y. M. Choi, M. L. Liu, and M. C. Lin, J. Phys. Chem. C **111**, 11117 (2007).
[27] X. Z. Yang, G. X. Luo, Z. S. Lu, and K. Hermansson, J. Chem. Phys. **127**, 074704 (2007).
[28] G. Kresse and J. Hafner, Phys. Rev. B **49**, 14251 (1994); G. Kresse and J. Furthmüller, Comput. Mater. Sci. **6**, 15 (1996).
[29] P. E. Blöchl, Phys. Rev. B **50**, 17953 (1994); G. Kresse and D. Joubert, *ibid.* **59**, 1758 (1999).
[30] J. P. Perdew, K. Burke, and M. Ernzerhof, Phys. Rev. Lett. **77**, 3865 (1996).
[31] D. R. Mullins, S. H. Overbury, and D. R. Huntley, Surf. Sci. **409**, 307 (1998).
[32] M. A. Henderson, C. L. Perkins, M. H. Engelhard, S. Thevuthasan, and C. H. F. Peden, Surf. Sci. **526**, 1 (2003).
[33] M. Methfessel and A. T. Paxton, Phys. Rev. B **40**, 3616 (1989).
[34] P. W. Tasker, J. Phys. C **6**, 488 (1980).

[35] P. M. Oliver, S. C. Parker, and W. C. Mackrodt, Modell. Simul. Mater. Sci. Eng. **1**, 755 (1993).
[36] E. Aneggi, C. de Leitenburg, G. Dolcetti, and A. Trovarelli, Catal. Today **114**, 40 (2006); E. Aneggi, J. Llorca, M. Maoro, and A. Trovarelli, J. Catal. **234**, 88 (2005).
[37] K. B. Zhou, X. Wang, X. M. Sun, Q. Peng, and Y. D. Li, J. Catal. **229**, 206 (2005).
[38] M. Nolan and G. W. Watson, J. Phys. Chem. B **110**, 16600 (2006).